Fusion of ^{28}Si + ^{28,30}Si: Different trends at sub-barrier energies

G. Montagnoli,[1] A. M. Stefanini,[2] H. Esbensen,[3] C. L. Jiang,[3] L. Corradi,[2] S. Courtin,[4] E. Fioretto,[2] J. Grebosz,[5] F. Haas,[4] H. M. Jia,[2] M. Mazzocco,[1] C. Michelagnoli,[1] T. Mijatović,[6] D. Montanari,[1] C. Parascandolo,[1] F. Scarlassara,[1] E. Strano,[1] S. Szilner,[6] and D. Torresi[1]

[1]*Dipartimento di Fisica e Astronomia, Università di Padova, and INFN, Sezione di Padova, I-35131 Padova, Italy*
[2]*INFN, Laboratori Nazionali di Legnaro, I-35020 Legnaro (Padova), Italy*
[3]*Physics Division, Argonne National Laboratory, Argonne, Illinois 60439, USA*
[4]*IPHC, CNRS-IN2P3, Université de Strasbourg, F-67037 Strasbourg Cedex 2, France*
[5]*Institute of Nuclear Physics, Polish Academy of Sciences, PL 31-342 Cracow, Poland*
[6]*Ruđer Bošković Institute, HR-10002 Zagreb, Croatia*

(Received 11 September 2014; published 20 October 2014)

Background: The fusion excitation function of the system ^{28}Si + ^{28}Si at energies near and below the Coulomb barrier is known only down to $\simeq$15 mb. This precludes any information on both coupling effects on sub-barrier cross sections and the possible appearance of hindrance. For ^{28}Si + ^{30}Si even if the fusion cross section is measured down to $\simeq$50 μb, the evidence of hindrance is marginal. Both systems have positive fusion Q values. While ^{28}Si has a deformed oblate shape, ^{30}Si is spherical.

Purpose: We investigate 1. the possible influence of the different structure of the two Si isotopes on the fusion excitation functions in the deep sub-barrier region and 2. whether hindrance exists in the Si + Si systems and whether it is strong enough to generate an S-factor maximum, thus allowing a comparison with lighter heavy-ion systems of astrophysical interest.

Methods: ^{28}Si beams from the XTU Tandem accelerator of the INFN Laboratori Nazionali di Legnaro were used. The setup was based on an electrostatic beam separator, and fusion evaporation residues (ER) were detected at very forward angles. Angular distributions of ER were measured.

Results: Fusion cross sections of ^{28}Si + ^{28}Si have been obtained down to $\simeq$600 nb. The slope of the excitation function has a clear irregularity below the barrier, but no indication of a S-factor maximum is found. For ^{28}Si + ^{30}Si the previous data have been confirmed and two smaller cross sections have been measured down to $\simeq$4 μb. The trend of the S-factor reinforces the previous weak evidence of hindrance.

Conclusions: The sub-barrier cross sections for ^{28}Si + ^{28}Si are overestimated by coupled-channels calculations based on a standard Woods-Saxon potential, except for the lowest energies. Calculations using the M3Y+repulsion potential are adjusted to fit the ^{28}Si + ^{28}Si and the existing ^{30}Si + ^{30}Si data. An additional weak imaginary potential (probably simulating the effect of the oblate ^{28}Si deformation) is required to fit the low-energy trend of ^{28}Si + ^{28}Si. The parameters of these calculations are applied to predict the ion-ion potential for ^{28}Si + ^{30}Si. Its cross sections are well reproduced by also including one- and successive two-neutron transfer channels, besides the low-lying surface excitations.

DOI: 10.1103/PhysRevC.90.044608 PACS number(s): 25.70.Jj, 24.10.Eq

I. INTRODUCTION

Fusion reactions are sensitive probes of the size and the nuclear structure properties of the reacting nuclei. In order to reveal this sensitivity it is important to compare the data for neighboring isotopes. The influence of transfer, for example, is clearly seen in the comparison of the fusion data for different nickel [1,2] and calcium isotopes [3]. The change of the structure from spherical vibrational to strongly deformed nuclei is clearly seen in the fusion of ^{16}O with different samarium isotopes [4,5].

In this work we discuss the fusion of the two silicon isotopes, ^{28}Si and ^{30}Si. They are particularly interesting because ^{30}Si is nearly spherical, whereas ^{28}Si is strongly deformed with an oblate shape. This difference has an interesting impact, as we shall see, on the energy dependence of the fusion cross sections at sub-barrier energies for the two symmetric systems ^{28}Si + ^{28}Si and ^{30}Si + ^{30}Si.

Another interesting question involves the influence of transfer on the fusion of the asymmetric system ^{28}Si + ^{30}Si. It is well known that couplings to pair-transfer channels with positive Q values can enhance the sub-barrier fusion cross section. It is therefore not unlikely that pair transfer could play a role in the fusion of ^{28}Si + ^{30}Si because the Q value is zero (elastic transfer).

Fusion of ^{28}Si + ^{28}Si [6] and of ^{30}Si + ^{30}Si [7] near and below the barrier is poorly known because existing data extend down to only $\approx$10 mb and the lowest 2 or 3 points show a considerable scatter for the lighter case. The cross sections for the fusion of ^{28}Si + ^{30}Si were measured by Jiang *et al.* [8] down to $\simeq$40 μb. The older data by Gary and Volant [6] cover higher energies, mostly above the Coulomb barrier, also for this system.

In this work we present the results of the full measurement of the excitation function of ^{28}Si + ^{28}Si from well below to well above the Coulomb barrier (a preliminary report on

 ©2014 American Physical Society

which was given in Ref. [9]) and of additional measurements for ^{28}Si + ^{30}Si, down to $\sigma_{\rm fus}$ of around 4μb. The data have been analyzed by coupled-channels (CC) calculations that are based on the M3Y+repulsion potential. Section II outlines the experimental setup and procedures, and the measured cross sections are presented. Section III describes the CC analyses for the symmetric systems ^{28}Si + ^{28}Si and ^{30}Si + ^{30}Si and the results are compared with the data. In Sec. IV the analysis is extended to the asymmetric system ^{28}Si + ^{30}Si where the effect of transfer is also discussed. Section V considers the possible hindrance behavior of ^{28}Si + ^{28,30}Si. The main results are summarized in Sec. VI.

II. SETUP AND RESULTS

The XTU Tandem accelerator of the Laboratori Nazionali di Legnaro of INFN provided ^{28}Si beams in the energy range of ≃46–86 MeV, with intensities of ≃15–30 pnA (up to 50 pnA in some cases). The targets were 50 μg/cm^2 metallic ^{28}Si and ^{30}SiO$_2$ evaporations on 15 μg/cm^2 carbon backings facing the beam. The isotopic enrichments were 99.93% and 96.50% for ^{28}Si and ^{30}Si, respectively. A very high enrichment was only necessary for the ^{28}Si targets because the heavier ^{29,30}Si stable isotopes produce Coulomb barriers lower than ^{28}Si in the laboratory system. The energy-dependent beam energy loss across the carbon backing and half of the silicon target was ≃750–850 keV, and it was taken into account in the analysis.

The evaporation residues (ER) were detected by using the setup schematically shown in Fig. 1 of Ref. [10]. The ER were separated from the beam by an electrostatic deflector. Subsequently, they were detected by two microchannel plate detectors, entered a transverse-field ionization chamber giving an energy loss (ΔE) signal, and were finally stopped in a circular 600 mm^2 silicon detector placed in the same gas (CH$_4$) volume. The silicon detector provided the residual energy E_r, as well as the start signal used for the times of flight, and triggered the data acquisition. More details can be found in Refs. [3,10].

Four silicon detectors were used for beam control and normalization. They were placed above and below and to the left and right of the beam at the same scattering angle $\theta_{\rm lab} = 16^\circ$ and measured the Rutherford scattering.

ER angular distributions were measured at $E_{\rm lab} = 58$, 67, 74, and 83.5 MeV in the range from $-8^{\rm o}$ to $+14^\circ$. They are rather wide, due to the evaporation of protons and α particles. Their width is constant at 58 and 67 MeV, and it starts increasing above. Total fusion cross sections were derived by integrating those distributions,and by simple interpolations or extrapolations for all other energies where ER measurements were taken only at 2° (or 3° for low energies).

The absolute cross section scale relies additionally on the knowledge of the relevant solid angles and of the transmission efficiency of the electrostatic deflector, $T = 0.72 \pm 0.04$, derived from several measurements performed for systems with similar mass asymmetries. Systematic errors on the absolute cross section scale sum up to an estimated ±7%, due to the geometrical solid angle uncertainties, to the angular distribution integrations, and to the transmission. Relative errors are basically determined by statistical uncertainties, which do not exceed 2%–3% near and above the barrier but are much larger at low energies where only a few fusion events could be detected.

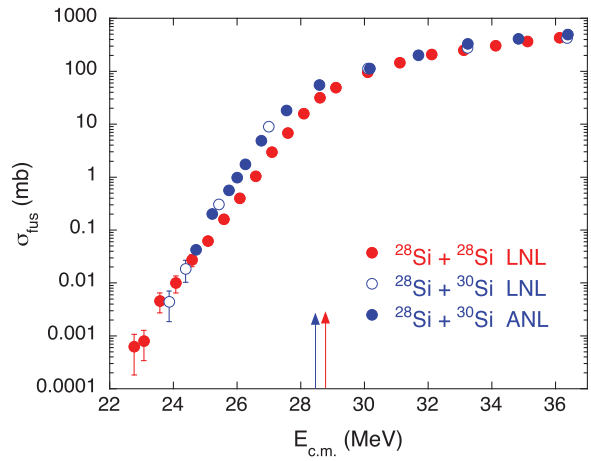

FIG. 1. (Color online) Excitation functions measured in this work for ^{28}Si + ^{28,30}Si, together with the previous data on ^{28}Si + ^{30}Si [8], obtained at Argonne (ANL). The arrows mark the positions of the Akyüz-Winther barriers [11] for the two systems.

The cross sections for ^{28}Si + ^{28}Si and ^{28}Si + ^{30}Si that we measured in this work, together with previous results [8] for the asymmetric system, are shown in Fig. 1. We can notice the good agreement between the two sets of data for ^{28}Si + ^{30}Si and the flatter slope for ^{28}Si + ^{28}Si. The two excitation functions actually cross each other at low energies. Figure 3 shows the logarithmic derivative of ^{28}Si + ^{28}Si. We notice a plateau below the barrier, and the slope seems to increase again at lowest energies without reaching the value expected for a constant astrophysical S factor.

III. COUPLED-CHANNELS CALCULATIONS

The coupled-channels calculations that are performed make use of the so-called rotating frame [12,13] or isocentrifugal [14] approximation, which simplifies the calculations by reducing the number of channels considerably. The calculations use either the M3Y+rep potential [15] or the standard Woods-Saxon potential of Ref. [11].

The densities of the reacting nuclei that determine the M3Y+rep potential are adjusted to optimize the fit to the fusion data. It is therefore convenient first to analyze the fusion data for the two symmetric systems ^{28}Si + ^{28}Si and ^{30}Si + ^{30}Si, because there are fewer parameters to adjust. In this approach, the diffuseness of both proton and neutron densities is kept fixed to $a = 0.48$ fm. The radius of the proton density is chosen to be consistent with the measured charge radius, whereas the radius of the neutron density is adjusted, and so is the diffuseness a_r associated with the repulsion (see Ref. [15] for details). The extracted densities are then applied in the next section to predict the M3Y+rep potential for the asymmetric system ^{28}Si + ^{30}Si.

TABLE I. The adopted coupling strengths for the excitation of the low-lying 2^+ and 3^- states in the two silicon isotopes. The structure input for the states in ^{28}Si and ^{30}Si is from Ref. [16]. The octupole strength of ^{30}Si is from Ref. [17]. The known quadrupole transitions from the first 2_1^+ state to the 0_2^+, 2_2^+, and 4_1^+ states are combined into a single quadrupole transition to an effective two-phonon state, denoted 2PH(2^+). The nucleus ^{28}Si is oblate [18] so the value of β_2 is negative. The nucleus ^{30}Si is spherical because the quadrupole moment of the 2_1^+ state is consistent with zero [18].

Nucleus	λ^π	E_x (MeV)	$B(E\lambda)$ (W.u.)	β_λ^C	β_λ^N
^{28}Si	2_1^+	1.779	13.2(3)	−0.411	−0.411
0–2:	0_2^+	4.980	8.6(16)		
4–2:	4_1^+	4.618	13.8(13)		
effective	2PH(2^+)	4.689	8.8	−0.238	−0.238
	3^-	6.879	13.9(24)	0.416	0.416
^{30}Si	2_1^+	2.235	8.5(11)	0.330	0.330
0–2:	0_2^+	3.787	≈1.4		
2–2:	2_2^+	3.499	9 (6)		
4–2:	4_1^+	5.279	4.7(13)		
effective	2PH(2^+)	4.331	5.2	0.184	0.184
	3^-	5.487	6.1 [17]	0.275	0.275

A. Structure input

The adopted coupling strengths for the excitation of the low-lying 2^+ and 3^- states in the two silicon isotopes are shown in Table I. It is assumed for simplicity, and because nothing better is known, that the β values are the same for Coulomb and nuclear-induced excitations. The nucleus ^{28}Si is assumed to have an oblate deformation whereas ^{30}Si is assumed to be spherical. The measured quadrupole moment of the 2^+ state in ^{28}Si is $Q_2 = 16(3)$ fm^2 [18], which determines the static deformation parameter $\beta_2^{\rm def} = -0.40(8)$. This is consistent with the β value $\beta_2 = -0.411$ obtained from the measured $B(E2)$ value shown in Table I. In contrast, the measured quadrupole moment of the 2^+ state in ^{30}Si is $Q_2 = -5(6)$ fm^2 [18]. This gives the prolate deformation parameter $\beta_2^{\rm def} = 0.12(14)$, but it is also consistent with a spherical nucleus.

B. Calculations and results

A complete CC calculation that includes all one- and two-phonon excitations as well as mutual excitations of the low-lying 2^+ and 3^- states in both projectile and target has 15 channels. In this work the mutual excitation of the 2^+ and 3^- states in the same nucleus is ignored and so are the excitations of states above 10 MeV. That eliminates the three two-phonon and mutual excitations of the 3^- states. The basic coupled-channels calculation has therefore 10 channels and is refereed to as Ch10. Such calculations are first performed for the fusion of the two symmetric systems ^{28}Si + ^{28}Si and ^{30}Si + ^{30}Si [7].

The calculations use the M3Y+rep potential and the densities of the reacting nuclei are adjusted as explained above to optimize the fit to the data. The results of the analysis for the two symmetric systems are compared to the data in Figs. 2(a) and 2(b). The slope for ^{28}Si + ^{28}Si is shown in Fig. 3.

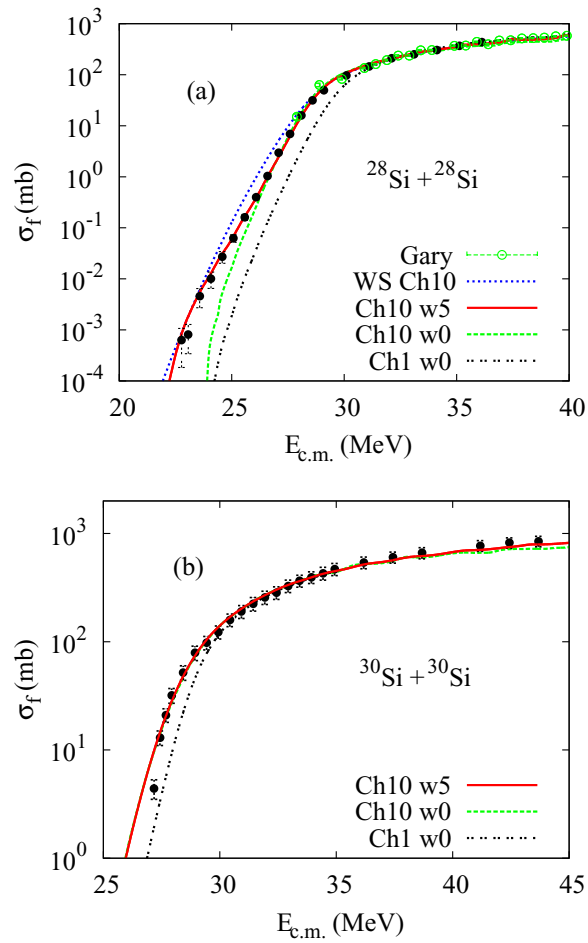

FIG. 2. (Color online) Cross sections for the fusion of ^{28}Si + ^{28}Si (this work and Ref. [6]) (a) and ^{30}Si + ^{30}Si [7] (b) compared to the no-coupling calculation Ch1 and to Ch10 coupled-channels calculations that are based on the M3Y+rep potential. A weak, short-ranged imaginary potential had to be applied (Ch10 w5, solid curve) in order to reproduce the low-energy data of ^{28}Si + ^{28}Si. Also shown in (a) is a Ch10 calculation that is based of a Woods-Saxon (WS) potential [11]. No imaginary potential was used in this case.

A surprising feature is that the low-energy data for ^{28}Si + ^{28}Si are best reproduced by applying a weak ($W_0 = 5$ MeV), short-ranged ($a_w = 0.2$ fm) imaginary potential, with a radius determined by the location of the minimum of the pocket in the entrance channel potential. The low-energy fusion of most heavy-ion systems, including the fusion hindrance phenomenon at very low energies, is usually best explained by ingoing-wave boundary conditions, without applying any imaginary potential. The need for an imaginary potential is possibly due to the strong oblate deformation of ^{28}Si, which causes the pocket minimum in the different reaction channel potentials to be located at different radial distances, as discussed below.

C. Channel potentials

The effect of deformation makes the channel potentials for the excited states in the two nuclei look very different.

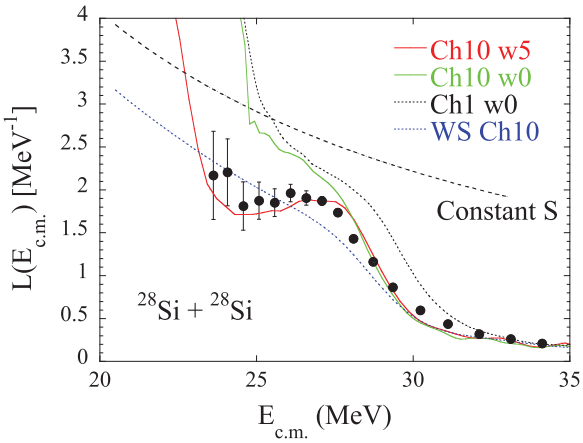

FIG. 3. (Color online) Logarithmic derivative (slope) of the excitation function of ^{28}Si + ^{28}Si as measured in this work. It is compared with the results of CC calculations [see also Fig. 2(a)] and with the slope expected for a constant astrophysical S factor ("Constant S"). The need for a weak imaginary potential is emphasized in this representation.

This can be seen in Fig. 4, where different channel potentials are illustrated for reactions of ^{28}Si + ^{30}Si. It is seen in Fig. 4(a) that the minimum of the channel potential for the 2^+ state in ^{28}Si is shifted to a smaller separation distance than observed in the entrance channel potential. This is due to the oblate deformation of ^{28}Si, which causes a nonzero quadrupole moment in the 2^+ channel. Since the incoming-wave boundary conditions (IWBC) are imposed at the minimum of the entrance channel potential, this implies that the fusion in the 2^+ channel is cut off at an energy that is higher than the minimum of the 2^+ channel potential. This behavior causes a suppression of the calculated cross sections for ^{28}Si + ^{28}Si at low energies, as illustrated by the (green) dashed curve in Fig. 2(a). However, by applying a weak imaginary potential it is possible to reproduce the low-energy data, as shown by the solid curve in Fig. 2(a).

The situation is different for the channels associated with the excited states of the spherical nucleus ^{30}Si. Here the minima of the channel potentials shown in Fig. 4(b) are located essentially at the same separation distance. The IWBC are therefore imposed at the minimum of each channel potential, which provides a more consistent treatment of the fusion in the different reaction channels. As a consequence, there is no need for an imaginary potential at low energy. This is illustrated for the fusion of ^{30}Si + ^{30}Si in Fig. 2(b), where the calculated cross sections are relatively insensitive to a weak imaginary potential at sub-barrier energies.

D. Densities

The densities of the silicon isotopes were parametrized in terms of the symmetrized Fermi function introduced in Ref. [19]. The parameters that were obtained from the analysis of the fusion data for the two symmetric systems are shown in Tables II and III. In the analysis of the ^{28}Si + ^{28}Si data it was assumed that the densities of protons and neutrons were the same, and the common radius of the densities and the

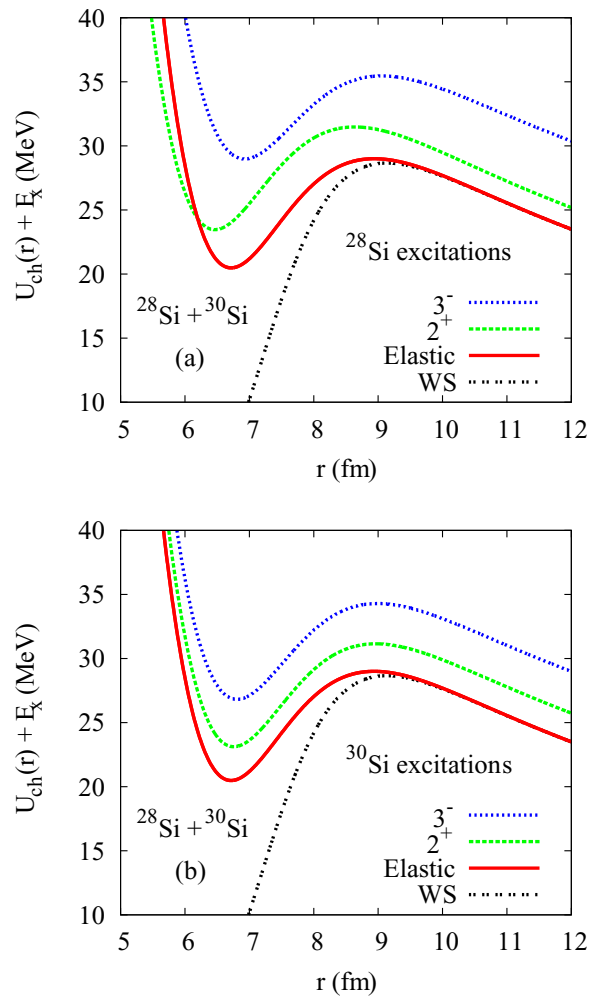

FIG. 4. (Color online) Channel potentials for ^{28}Si + ^{30}Si. The solid curve is the M3Y+rep entrance channel potential. Also shown are channel potentials for the 2^+ and 3^- excited states in ^{28}Si (a) and in ^{30}Si (b). The channel potentials were calculated for $L = 0$ with the parameters shown in Tables II and III; they have been displaced by the excitation energies E_x. The entrance channel potential for the adjusted Woods-Saxon (WS) potential mentioned in Table II is also shown.

diffuseness a_r associated with the repulsion were adjusted to optimize the fit to the present fusion data. The strength of the repulsion (v_r) was calibrated as explained in Ref. [15] to produce a nuclear incompressibility of $K = 234$ MeV as predicted for $N = Z$ nuclei by Myers and Świątecki [20].

The rms radius of the ^{28}Si density obtained from the analysis of the fusion data is shown in Table III. It is seen to be in very good agreement with the rms radius of the point-proton distribution that has been extracted from the measured rms charge radius [21].

Since the neutron and proton densities of ^{30}Si could be different, a point-proton density that is consistent with the measured charge radius of ^{30}Si was adopted. The radius of the neutron density was adjusted together with the diffuseness associated with the repulsion to optimize the fit to the ^{30}Si + ^{30}Si fusion data of Ref. [7]. The optimization was performed

TABLE II. Results of the analysis of the Si + Si fusion data. The analysis of the data for ^{28}Si + ^{28}Si and ^{30}Si + ^{30}Si [7] included 10 channels and employed an imaginary potential with the parameters $W_0 = 5$ MeV and $a_w = 0.2$ fm and a radius determined by the minimum of the pocket in the entrance channel potential. The lowest data point of Ref. [7] was excluded, and a systematic error of 5% was included in the analysis of the ^{28}Si + ^{28}Si data. The diffuseness a_r and the radius R_n of the neutron density that determine the M3Y+rep potential were adjusted to minimize χ^2/N, whereas the radius of the proton density, R_p, is consistent with the rms charge radius (see Table III). For the asymmetric ^{28}Si + ^{30}Si system, the a_r, R_p, and R_n parameters were predicted by the values obtained for the two symmetric systems. The calculations included either 10 or 30 channels as explained in the text. The data of Refs. [6,7] were also analyzed using a standard Woods-Saxon (WS) potential [11] and the radius of the potential was adjusted in each case (see the third column) to optimize the fit to the data.

Reaction	a_r (fm)	R_p (fm)	R_n (fm)	$V_{\min}$ (MeV)	V_{CB} (MeV)	χ^2/N	Data Ref.
^{28}Si + ^{28}Si Ch10w5	0.398	3.135	3.135	23.76	29.37	1.71	
^{30}Si + ^{30}Si Ch10w5	0.380	3.165	3.216	17.65	28.67	0.36	[7]
^{28}Si + ^{30}Si Ch10w5		predicted		20.48	29.00	7.34	[8]
^{28}Si + ^{30}Si Ch10w5 ($\Delta E = -0.2$ MeV)		predicted				1.82	[8]
^{28}Si + ^{30}Si Ch30w5		predicted		20.48	29.00	1.39	[8]
^{28}Si + ^{28}Si Ch10w0 WS		6.980		2.05	29.24	1.29	[6]
^{28}Si + ^{30}Si Ch30w0 WS		7.110		0.27	28.74	1.78	[6]
^{30}Si + ^{30}Si Ch10w0 WS		7.132		−0.61	28.61	0.28	[7]

with the constraint that the nuclear incompressibility was fixed at $K = 232.7$ MeV [20], which was achieved (see Ref. [15]) by adjusting v_r.

The result of the analysis shows that the rms radius of neutrons is only 0.032 fm larger than the rms radius of the point protons. This result is consistent with the trend of the experimental neutron skin thickness obtained from antiproton experiments [22].

IV. FUSION OF THE ASYMMETRIC SYSTEM ^{28}Si + ^{30}Si

The previous data on ^{28}Si + ^{30}Si [8] were already nicely reproduced by CC calculations using the M3Y+repulsion potential and the low-lying excited states of ^{28}Si and ^{30}Si. In that case however the potential parameters were simply adjusted to get the best data fit.

A better approach has been pursued in this work, where the densities of the silicon isotopes determined in the previous section have been applied to predict the ion-ion potential for the asymmetric system ^{28}Si + ^{30}Si. The only parameter that is missing is the strength of the repulsion, $V_{\rm rep}$, but that is determined to produce a nuclear incompressibility $K = 233.37$ MeV, which is the value predicted for the compound nucleus ^{58}Ni [20]. The channel potentials one obtains are shown in Fig. 4.

The Ch10 calculation, which is similar to the calculations for the symmetric systems, gives a rather poor fit to the data for ^{28}Si + ^{30}Si, as shown in Table II. The fit to the data can be improved considerably simply by shifting the calculated cross sections 200 keV to lower energies. There is possibly some important reaction mechanism missing which could explain this shift. The most obvious candidate is neutron transfer, because the ground-state Q value for one-neutron transfer is only −2.135 MeV and the exchange of two neutrons can occur with a Q value of 0 MeV.

The influence of the one- and two-neutron transfer reactions that are built on the Ch10 surface excitations discussed above is calculated by using the model developed in Ref. [23]. In the model excitations and transfer are assumed to be independent degrees of freedom. This implies that the excitation spectrum in Table I is the same for all mass partitions. A calculation that includes 10 excitation channels, a one-neutron transfer, followed by a second, successive neutron transfer, will therefore have 30 channels and is denoted Ch30.

The coupling to the one-neutron transfer is constructed from the so-called Quesada form factors [26] by using the spectroscopic factors shown in Table IV. The form factors for the different one-neutron transfer channels are combined into

TABLE III. Density parameters for ^{28}Si and ^{30}Si. The point-proton rms radii [rms(pp)] were obtained from the measured rms charge radii, rms(ch), of Ref. [21]. The parameters of the proton densities, the radius R, and the fixed diffuseness $a = 0.48$ fm that reproduce point-proton rms radii are shown. The parameters of the neutron densities that were determined in the analysis of the fusion data for the two symmetric systems, ^{28}Si + ^{28}Si and ^{30}Si + ^{30}Si [7], are also shown.

Source	R (fm)	a (fm)	rms (fm)	rms(pp) (fm)	rms(ch) (fm)
^{28}Si	3.142	0.48	3.018	3.018(2)	3.122(2)
fusion	3.135	0.48	3.013		
^{30}Si	3.165	0.48	3.032	3.032(4)	3.133(4)
fusion	3.216	0.48	3.064		

TABLE IV. Spectroscopic factors for one-neutron pickup by ^{28}Si (Table IV of Ref. [24]) and stripping from ^{30}Si (Table 29.15 of Ref. [25]). The ground-state Q value for the one-neutron transfer is −2.135 MeV.

Nucleus	state	E_x (MeV)	^{28}Si(d,p)	^{30}Si(p,d)
^{29}Si	$2s_{1/2}$	0	0.32	0.78
^{29}Si	$1d_{3/2}$	1.273	0.69	0.77
^{29}Si	$1d_{5/2}$	2.032	0.16	1.8

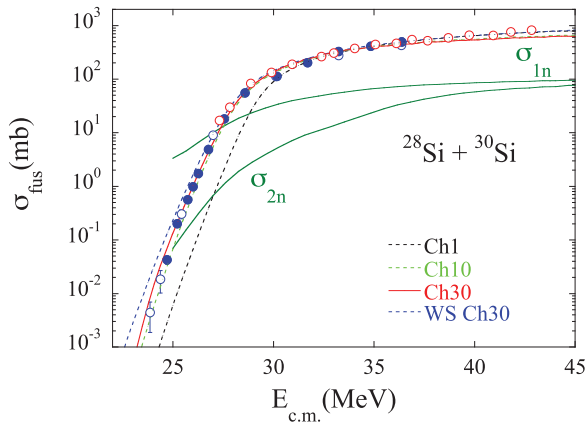

FIG. 5. (Color online) Fusion cross sections for ^{28}Si + ^{30}Si (with previous data from [6,8]) compared to the no-coupling Ch1 calculation and to Ch10 and Ch30 coupled-channels calculations that are based on a Woods-Saxon (WS) potential and the predicted M3Y+rep potential. No imaginary potential was used. The one- and successive two-neutron transfer cross sections, σ_{1n} and σ_{2n}, obtained in Ch30 calculations are also shown.

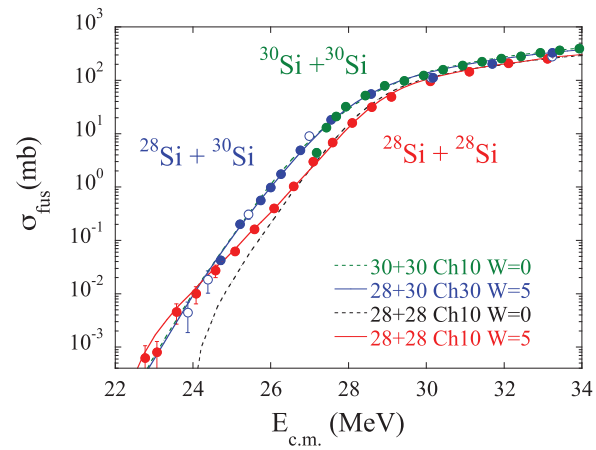

FIG. 6. (Color online) Measured fusion cross sections for ^{28}Si + ^{28}Si and ^{30}Si + ^{30}Si [7] compared to Ch10 calculations, and the data for ^{28}Si + ^{30}Si compared to Ch30 calculations. All calculations are based on M3Y+rep potentials. Note that it is necessary to use an imaginary potential with parameters $a_w = 0.2$ fm and $W_0 = 5$ MeV in order to reproduce the ^{28}Si + ^{28}Si data at low energy.

one effective transfer coupling, as described in Ref. [23]. The effective Q value for the one-neutron transfer is set equal to the ground-state Q value of -2.315 MeV. This would be the correct choice if the transfer from the $s_{1/2}$ orbit of ^{30}Si to the $1/2^+$ ground state of ^{29}Si dominated. However, the transfer can also leave the produced ^{29}Si nuclei in excited states, as shown in Table IV. To compensate for that, the strength of the transfer coupling was multiplied with a simple scaling factor, which was adjusted to optimize the fit to the fusion data. The necessary scaling factor was found to be 0.912.

The results of the Ch30 calculations described above are compared to the data in Fig. 5. The data are suppressed or hindered at low energies compared to the calculation that uses a Woods-Saxon potential. The radius of the Woods-Saxon well was adjusted to provide an optimum fit to the high-energy data of Gary and Volant [6]. The Ch30 calculation that uses the predicted M3Y+rep potential provides a good description of the sub-barrier data, with a χ^2/N value of the order of 1 to 2. The predicted one- and (successive) two-neutron cross sections are also shown in the figure.

The fusion cross sections for the three combinations of the silicon isotopes are compared in Fig. 6. In this connection, it is very unfortunate that the cross sections for ^{30}Si + ^{30}Si measured by Bozek *et al.* [7] did not reach very small values but stopped at 4.4 mb. This situation has some analogies to the fusion of the two nickel isotopes ^{58}Ni and ^{64}Ni discussed in Refs. [1,2] and of the two calcium isotopes ^{40}Ca and ^{48}Ca that were discussed in Ref. [3]. The measured fusion cross section for those asymmetric systems are enhanced with respect to the corresponding symmetric cases.

The enhancement was explained by the influence of couplings on transfer channels. This reaction mechanism also plays some role in the fusion of the asymmetric silicon system but it is not very strong according to the calculations shown in Fig. 5.

V. HINDRANCE OR NO HINDRANCE

One of the goals of this work was to investigate the hindrance of fusion in Si + Si systems at very low energies and determine whether the S factor for fusion develops a maximum at energies that are accessible to experiments. The S factor does not necessarily have to develop a maximum because the Q value for fusion is positive (being 13.4 MeV for ^{28}Si + ^{30}Si). It is only when the Q value is negative that the S factor must have a maximum because the cross section must vanish if the center-of-mass energy is less than the positive energy where the compound nucleus is produced in its ground state [27].

The S factors for the fusion of ^{28}Si + ^{28}Si are shown in Fig. 7(a). It is seen that the data are indeed hindered at energies that are slightly below the Coulomb barrier ($V_{CB} \approx$ 29.4 MeV) compared to the calculation that uses the Woods-Saxon potential. However, the hindrance disappears at even lower energies, near 23 MeV. This type of behavior has to our knowledge never been observed before. The data are poorly reproduced by calculations that use the M3Y+rep potential and ingoing-wave boundary conditions to simulate the fusion (see the green dashed curve). In order to reproduce the data it is necessary to apply a weak, short-ranged imaginary potential, as illustrated by the solid curve in Fig. 7(a).

The measured fusion cross sections for ^{28}Si + ^{30}Si are also hindered just a few MeV below the Coulomb barrier compared to the calculation that uses a standard Woods-Saxon potential. This is shown in Fig. 7(b). The hindrance persists in this case and grows as the beam energy is reduced further. The data are reproduced fairly well by applying the M3Y+rep potential and ingoing-wave boundary conditions to determine the fusion. The calculation Ch30, which includes the effect of neutron transfer as explained earlier, does a slightly better job than the Ch10 calculation in reproducing the data. It produces a plateau of constant S factors, between 21 and 24 MeV. It appears that the data develop a similar plateau below 25 MeV. In fact, an

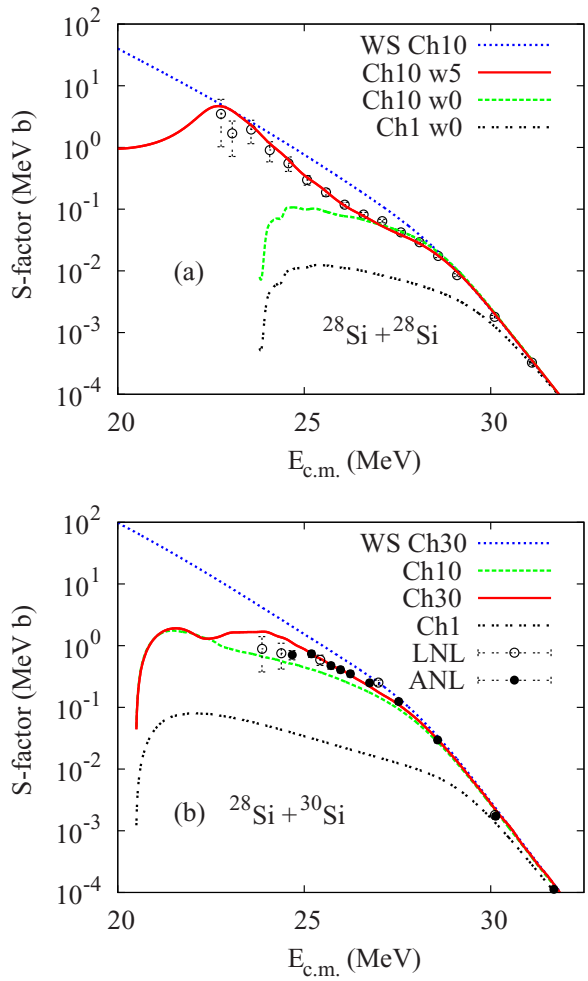

FIG. 7. (Color online) S factors for the fusion of ^{28}Si + ^{28}Si (a) and ^{28}Si + ^{30}Si (b). A weak imaginary potential ($a_w = 0.2$ fm $W_0 = 5$ MeV) was used in the Ch10 w5 calculation of the fusion of ^{28}Si + ^{28}Si.

extrapolation of the ANL data [8] suggests that a maximum S factor is expected to appear at 24.2 ± 3.6 MeV (see Table I in Ref. [28].)

It is clear that a hindrance of the fusion does occur for both systems discussed in this section in the sense that the data are suppressed compared to calculations that use a conventional Woods-Saxon potential. However, it is still unclear whether a well-defined maximum of the S factor exists for the fusion of ^{28}Si + ^{30}Si or whether it will develop if the measurements were pushed to even lower energies. The two new, low-energy data points labeled LNL in Fig. 7(b) are consistent with the previous ANL data of Ref. [8], but they do not resolve the issue of a maximum S factor because the error bars are large.

It would also be very interesting to push the measurements for ^{28}Si + ^{28}Si to even lower energies to investigate the abnormal behavior of the S factor for the fusion of this system, which is possibly linked to the relatively strong oblate deformation of both projectile and target.

VI. SUMMARY

The fusion excitation function of ^{28}Si + ^{28}Si has been extended in a wide range down to ≃600 nb. We observe a clear irregularity of its slope below the barrier. However, we have no indication of an S-factor maximum in the measured energy range. Further measurements have been performed for ^{28}Si + ^{30}Si, confirming the previous data and adding two smaller cross sections down to ≃4 μb. The trend of the S factor in this case supports the previous weak evidence of hindrance.

Coupled-channels calculations based on a standard Woods-Saxon potential overestimate the sub-barrier cross sections of ^{28}Si + ^{28}Si, which is an indication of the hindrance phenomenon, but this effect disappears at the lowest energies. The oblate deformation of ^{28}Si may be the cause of this behavior, which has never been observed before to our knowledge. Coupled-channels calculations have been performed using the M3Y potential by adjusting its parameters to fit the ^{28}Si + ^{28}Si and the existing ^{30}Si + ^{30}Si data. This has allowed us to predict the M3Y+rep potential for the asymmetric system ^{28}Si + ^{30}Si.

The results of the calculations for the two symmetric systems are good. However, it is surprising that the low-energy data for ^{28}Si + ^{28}Si are best reproduced by applying a weak, short-ranged imaginary potential, probably simulating the effect of the oblate deformation. This feature has to be further investigated. The full excitation function of ^{28}Si + ^{30}Si is nicely fitted. The best result is obtained by including one- and successive two-neutron transfer channels in the coupling scheme, besides the low-lying surface excitations.

ACKNOWLEDGMENTS

We are very grateful to the XTU Tandem staff and to M. Loriggiola for preparing targets of excellent quality. The research leading to these results has received funding from the European Union Seventh Framework Programme FP7/2007-2013 under Grant Agreement No. 262010–ENSAR. This work has been supported in part by the Croatian Science Foundation under the project 7194. H.E. is supported by the US Department of Energy, Office of Science, Office of Nuclear Physics, Contract No. DE-AC02-06CH11357.

[1] M. Beckerman, M. Salomaa, A. Sperduto, J. D. Molitoris, and A. Di Rienzo, Phys. Rev. C **25**, 837 (1982).
[2] M. Beckerman *et al.*, Phys. Rev. Lett. **45**, 1472 (1980).
[3] G. Montagnoli *et al.*, Phys. Rev. C **85**, 024607 (2012).
[4] R. Stokstad *et al.*, Z. Phys. A **295**, 269 (1980).
[5] H. Esbensen, Nucl. Phys. A **352**, 147 (1982).
[6] S. Gary and C. Volant, Phys. Rev. C **25**, 1877 (1982).
[7] E. Bozek *et al.*, Nucl. Phys. A **451**, 171 (1986).
[8] C. L. Jiang *et al.*, Phys. Rev. C **78**, 017601 (2008).
[9] A. M. Stefanini *et al.*, EPJ Web Conf. **66**, 03082 (2014).
[10] A. M. Stefanini *et al.*, Phys. Rev. C **82**, 014614 (2010).
[11] A. Winther, Nucl. Phys. A **594**, 203 (1995).
[12] O. Tanimura, Phys. Rev. C **35**, 1600 (1987).

[13] H. Esbensen, S. Landowne, and C. Price, Phys. Rev. C **36**, 1216 (1987).
[14] J. Gomez-Comacho and R. C. Johnson, J. Phys. G **12**, L235 (1986).
[15] Ş. Mişicu and H. Esbensen, Phys. Rev. C **75**, 034606 (2007).
[16] ENSDF, NNDC, Brookhaven National Laboratory, www.nndc.bnl.gov/ensdf
[17] R. H. Spear, At. Data Nucl. Data Tables **42**, 55 (1989).
[18] N. J. Stone, At. Data Nucl. Data Tables **90**, 75 (2005).
[19] H. Esbensen and Ş. Mişicu, Phys. Rev. C **76**, 054609 (2007).
[20] W. D. Myers and W. J. Świątecki, Phys. Rev. C **62**, 044610 (2000).
[21] I. Angeli, At. Data Nucl. Data. Tables **87**, 185 (2004).
[22] A. Trzcińska, J. Jastrzebski, P. Lubinski, F. J. Hartmann, R. Schmidt, T. von Egidy, and B. Klos, Phys. Rev. Lett. **87**, 082501 (2001).
[23] H. Esbensen, C. L. Jiang, and K. E. Rehm, Phys. Rev. C **57**, 2401 (1998).
[24] R. J. Vojtech *et al.*, Phys. Rev. C **35**, 2139 (1987).
[25] P. M. Endt and C. Van der Leun, Nucl. Phys. A **310**, 1 (1978).
[26] J. M. Quesada, G. Pollarolo, R. A. Broglia, and A. Winther, Nucl. Phys. A **442**, 381 (1985).
[27] C. L. Jiang, B. B. Back, H. Esbensen, R. V. F. Janssens, and K. E. Rehm, Phys. Rev. C **73**, 014613 (2006).
[28] B. B. Back, H. Esbensen, C. L. Jiang, and K. E. Rehm, Rev. Mod. Phys. **86**, 317 (2014).